Noname manuscript No.
(will be inserted by the editor)

Modified geometry of spur gear drives for compensation of shaft deflections

Ignacio Gonzalez-Perez · Victor Roda-Casanova · Alfonso Fuentes

Received: date / Accepted: date

Abstract One of the greatest concern of spur gears is the edge contact of tooth surfaces that is caused by misalignment of the gear drive. Such a misalignment is caused partially by the deflections of the shafts where the gears are mounted. As a result of the edge contact a non favorable condition of bearing contact is achieved, providing a high level of contact and bending stresses. An intensive research and many practical solutions have been directed to modify the gear tooth surfaces in order to avoid edge contact. An innovative procedure is proposed here for: (i) determination of the errors of alignment at the gear drive caused by shaft deflections, (ii) incorporation of such errors of alignment in the generation process of spur gears for compensation of shaft deflections, and (iii), determination of a favorable function of transmission errors for the design load. A finite element model of a spur gear drive including pinion and wheel shafts is used for the determination of the errors of alignment along the cycle of meshing. Compensation of misalignments in gear generation is then accomplished by modification of pinion tooth surfaces whereas the wheel tooth surfaces are kept unmodified. Additional modifications of pinion tooth surfaces may be required for the obtention of a favorable function of transmission errors. The effect of several misalignment compensations in the reduction of contact stresses has been investigated. Postprocessing of load intensity functions and loaded transmission errors is included. The developed approach is illustrated with numerical examples.

Ignacio Gonzalez-Perez
Polytechnic Universtiy of Cartagena
Department of Mechanical Engineering
Campus Muralla, Dr. Fleming s/n, 30202 Cartagena
Murcia, Spain
Tel.: +34-968326429
Fax: +34-968326449
E-mail: ignacio.gonzalez@upct.es

Victor Roda-Casanova
Universitat Jaume I, Castellon, Spain

Alfonso Fuentes
Polytechnic University of Cartagena, Spain

Keywords gear geometry · tooth contact analysis · finite element analysis · loaded transmission errors · shaft deflections

1 Introduction

Spur gear drives are widely applied in the industry and have been a focus of intensive research to improve the load capacity and the conditions of meshing of involute profiles. First modifications on involute profiles, proposed in [1], were directed to remove some material from the borders of the tooth surfaces in order to minimize transmission errors for the design load. Many contributions in this area have been done [2, 3, 4, 5, 6] looking for gear drives with reduced noise and vibration. Substitution of involute profile by other types of profiles has been another topic of intensive research. A pair of circular profiles for the generating cutters was proposed in [7] and mismatch of the circular profiles of the cutters was proposed for localization of the bearing contact in [8]. Modification of pinion tooth surfaces by application of parabolic profiles instead of straight profiles of the cutters has been proposed in [9] for the localization of the bearing contact. Localization of the bearing contact by the application of mismatched profiles of the cutters makes the contact less sensitive to the errors of alignment but, at the same time, increase contact and bending stresses, and transmission errors.

A double crowned pinion tooth surface has been proposed in [10] for the localization of the bearing contact and the predesign of a parabolic function of unloaded transmission errors that control the transfer of meshing between adjacent pairs of teeth. A compromise solution was found in [11] combining a straight profile for the main part of the cutter tooth surface surrounded by parabolic profiles at the borders of the cutter tooth surfaces. This partial crowning keeps an involute area with no modification and allows: (i) reduction of the sensitivity of the bearing contact when errors of alignment are present, (ii) reduction of contact and bending stresses respect to a whole crowned tooth surface or respect to an involute tooth surface when errors of alignment are present, and (iii) reduction of unloaded transmission errors when misalignments are lower.

The determination of the appropriate topology of the gear tooth surfaces may not have a only solution. One of the main problems that may cost the shift of the bearing contact on the gear tooth surfaces is the deflection of the shafts where the gears are mounted, specially when the gears are installed out of the middle location between bearings. The deflection of the shafts implies then a misalignment of the wheel respect to the pinion and, consequently, the shift of the bearing contact. The main goal of this paper is to consider the shaft deflections, due to the design load, in the determination of the pinion tooth surface that provides, under misalignment, an almost conjugate action with the wheel tooth surface. This idea will allow to get a uniform distributed bearing contact for the design load. However, the bearing contact will be shifted when the load is far from the design load. Some additional modifications of the obtained pinion tooth surface may be required for the reduction of the sensitivity of the shift of the bearing contact and the reduction of transmission errors.

More specifically, the presented research has the following goals:

(1) Presentation of a method for determination of shaft deflections along the cycle of meshing between a pair of gears mounted on their corresponding shafts.
(2) Generation of the pinion tooth surface in misaligned conditions in order to have almost linear contact under the design load. The obtained geometry in misaligned condition is called compensated geometry.
(3) Determination of load intensity functions at every contact position of the cycle of meshing and comparison of such functions provided by the standard geometry, based on involute profiles, and the compensated geometry.
(4) Determination of loaded transmission errors along the cycle of meshing and modification of the compensated geometry to provide it with a predesign function of unloaded transmission errors. The predesign function of unloaded transmission errors will help reducing the resulting level of transmission errors.

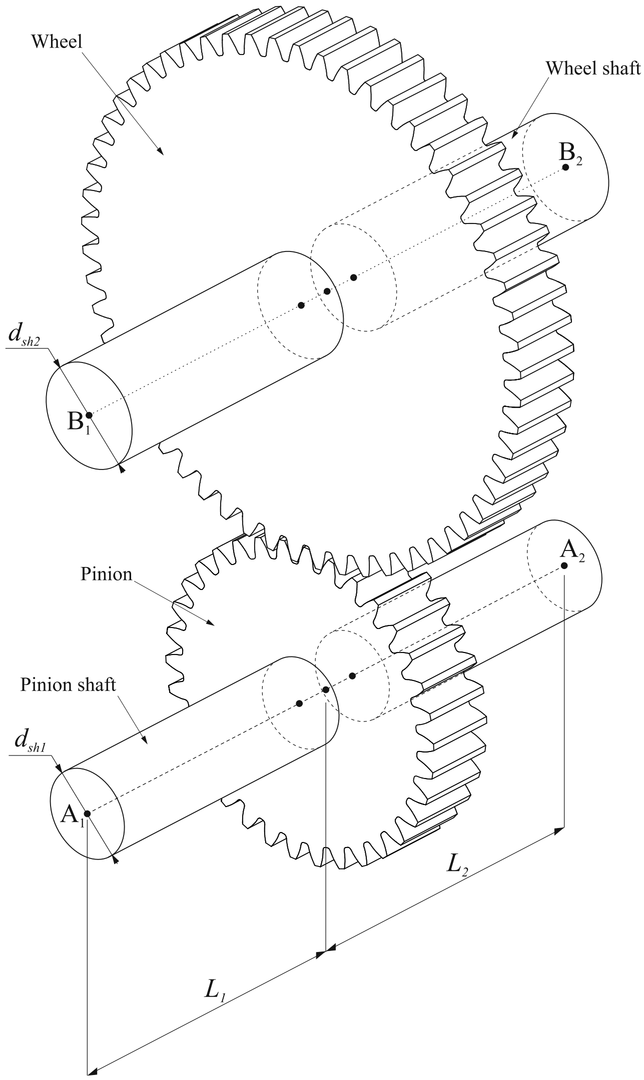

Fig. 1 Physical model of the gear drive

The developed research is illustrated with numerical examples and has been applied to the physical model shown in Fig. 1. The physical model is based on two gears mounted in their corresponding shafts. The gears may be mounted out of the middle location between bearings by modifying lengths L_1 and L_2. This means that shaft deflections due to the design load will cost misalignment between pinion and wheel. A finite element model of the physical model shown in Fig. 1 has been built considering the ideas proposed in [12] for the development of the presented research.

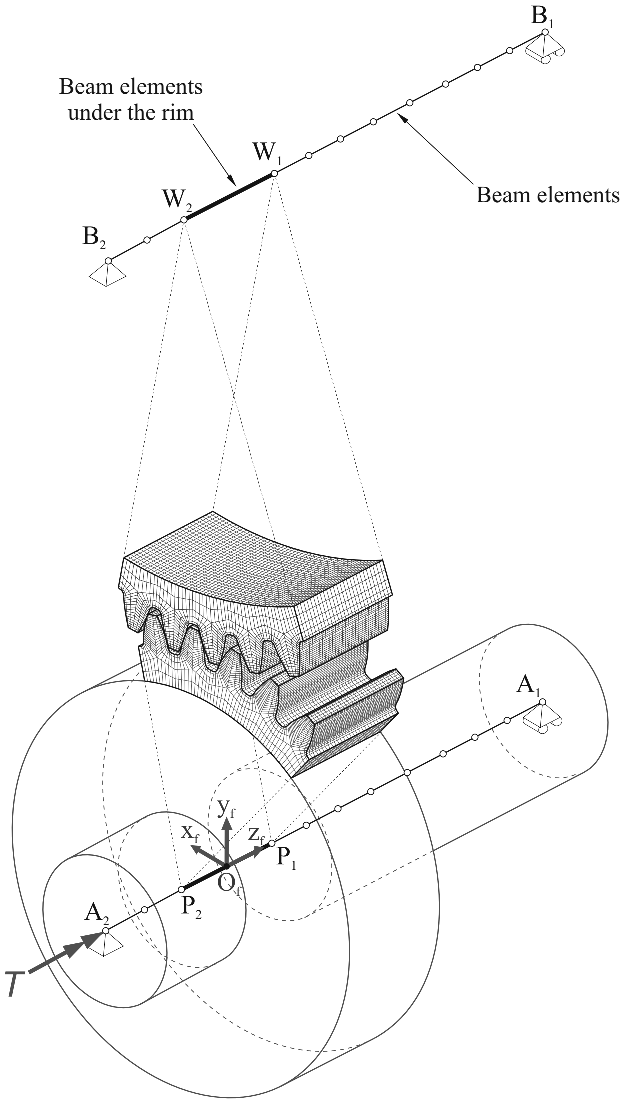

Fig. 2 Scheme of the finite element model

2 Determination of gear misalignments due to shaft deflections

Figure 2 shows schematically the finite element model of the physical model shown in Figure 1. Linear beam elements are considered for the modeling of shaft deflections. The transversal area of the shafts is considered as a property of the beam elements. For the portions of the shafts located under the pinion and wheel rims, the transversal area of the beam elements covers up to the bottom part of the rims. Torsional deformation is considered by modeling of rigid edges on the rim rigidly connected to the nodes of the beam elements that are located under the rim. A design load is applied by means of a torque T at bearing A_2 while the rotation of the wheel shaft is blocked at node B_2. More details of the schematic model shown in Figure 2 can be found in [12].

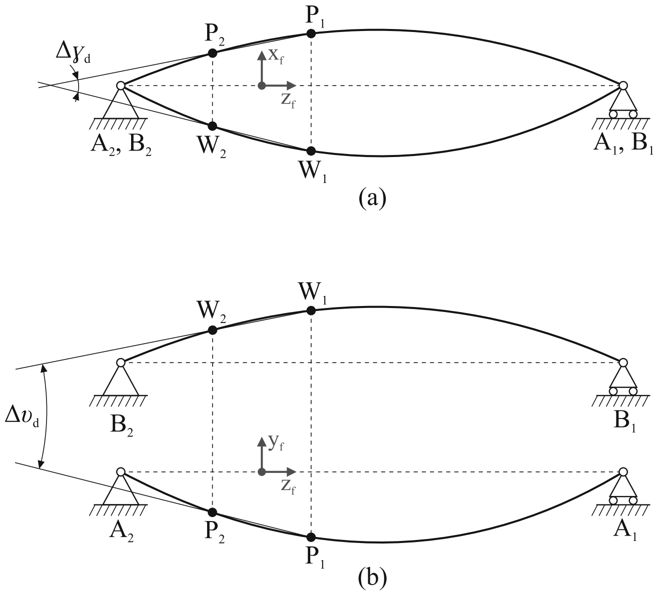

Fig. 3 For determination of misalignments $\Delta\gamma_d$ and $\Delta\nu_d$ due to shaft deflections

The misalignment between pinion and wheel is determined from the displacements that reference nodes $P1$, $P2$, $W1$, and $W2$ (see Fig. 2) experiment for the design load T at each given contact position. The whole cycle of meshing is considered though a certain number of contact positions. The displacements (u_{xi}, u_{yi}, u_{zi}) are obtained from the results of the finite element analysis for each contact position i and are represented in the fixed coordinate system S_f, shown in Fig. 2. Mean values $(\overline{u}_x, \overline{u}_y, \overline{u}_z)$ are then determined at each reference node for the whole cycle of meshing.

The misalignment due to the tangential loading between the gear tooth surfaces is considered through the magnitude $\Delta\gamma_d$, shown in Fig. 3(a). Here, subindex d means *deflection*, since shaft deflection costs the misalignment. Such a magnitude is determined as

$$\Delta\gamma_d = \arctan\left[\frac{\overline{u}_x^{(W1)} - \overline{u}_x^{(W2)}}{b_w}\right] - \arctan\left[\frac{\overline{u}_x^{(P1)} - \overline{u}_x^{(P2)}}{b_p}\right] \quad (1)$$

where b_p and b_w are the pinion and wheel face widths, respectively.

The misalignment due to the radial loading between the gear tooth surfaces is considered through the magnitude $\Delta\nu_d$, shown in Fig. 3(b). Such a magnitude is determined as

$$\Delta\nu_d = \arctan\left[\frac{\overline{u}_y^{(W1)} - \overline{u}_y^{(W2)}}{b_w}\right] - \arctan\left[\frac{\overline{u}_y^{(P1)} - \overline{u}_y^{(P2)}}{b_p}\right] \quad (2)$$

The relative displacements of the wheel respect to the pinion are considered through magnitudes Δx_d, Δy_d,

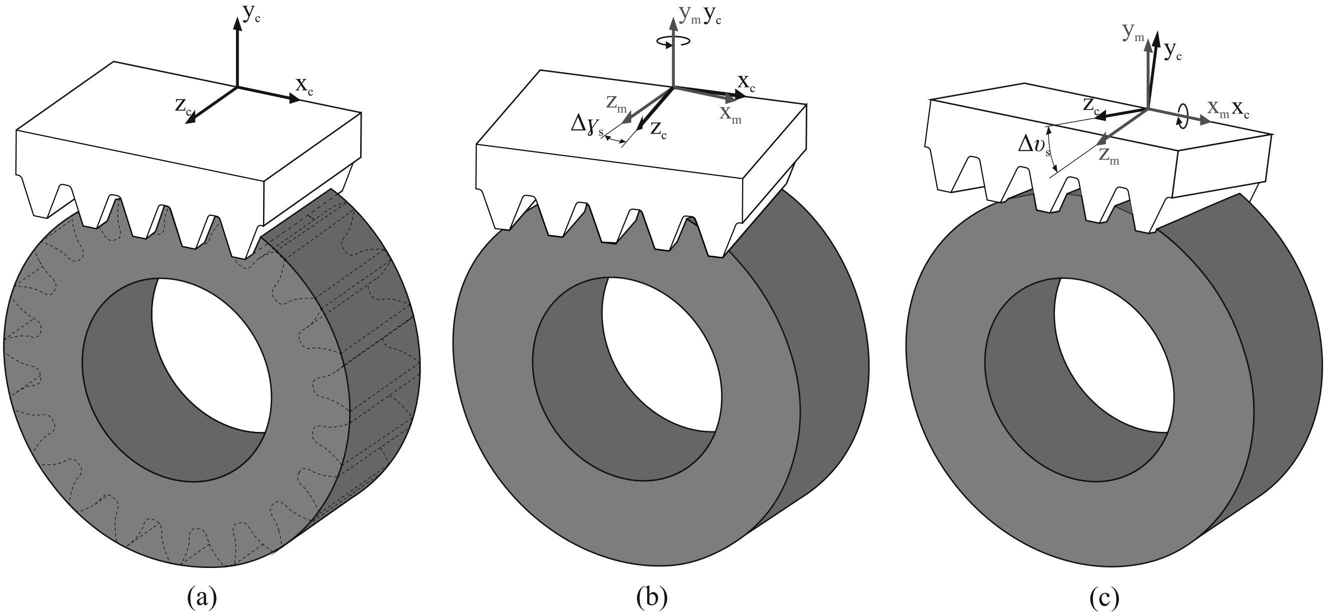

Fig. 4 Installment of the rack-cutter in: (a) a standard setting, (b) a setting with $\Delta\gamma_s$, and (c) a setting with $\Delta\nu_s$

and Δz_d, and are obtained as

$$\Delta x_d = \left[\frac{\overline{u}_x^{(W1)} + \overline{u}_x^{(W2)}}{2}\right] - \left[\frac{\overline{u}_x^{(P1)} + \overline{u}_x^{(P2)}}{2}\right] \tag{3}$$

$$\Delta y_d = \left[\frac{\overline{u}_y^{(W1)} + \overline{u}_y^{(W2)}}{2}\right] - \left[\frac{\overline{u}_y^{(P1)} + \overline{u}_y^{(P2)}}{2}\right] \tag{4}$$

$$\Delta z_d = \left[\frac{\overline{u}_z^{(W1)} + \overline{u}_z^{(W2)}}{2}\right] - \left[\frac{\overline{u}_z^{(P1)} + \overline{u}_z^{(P2)}}{2}\right] \tag{5}$$

3 Gear generation

Gear tooth surfaces can be analytically determined from any cutter regular tooth surface following the modern theory of gearing [13]. Two coordinate systems S_c and S_1 are considered rigidly connected to the cutter and the pinion tooth surfaces. Coordinate transformation from system S_c to system S_1 and observation of the equation of meshing allow the pinion tooth surface to be determined from the rack-cutter tooth surface

$$\mathbf{r}_1(u,v,\psi) = \mathbf{M}_{1c}(\psi_1)\mathbf{r}_c(u,v) \tag{6}$$

$$\left(\frac{\partial \mathbf{r}_1}{\partial u} \times \frac{\partial \mathbf{r}_1}{\partial v}\right) \cdot \frac{\partial \mathbf{r}_1}{\partial \psi} = 0 \tag{7}$$

Here, (u,v) are the cutter surface parameters and ψ is the generalized parameter of generation. Matrix $\mathbf{M}_{1c}$ allows coordinate transformation from system S_c to system S_1. Simultaneous consideration of equations 6 and 7 allows pinion tooth surface to be determined.

Figure 4(a) shows the standard setting of a rack-cutter over the pinion being generated. Settings of the rack-cutter with angular magnitudes $\Delta\gamma_s$ and $\Delta\nu_s$ are shown in Figures 4(b) and 4(c), respectively. Here, coordinate system S_m is an auxiliary fixed coordinate system that is parallel to system S_f (see Fig.2). System S'_c is an auxiliary coordinate system parallel to system S_c, not shown in Fig. 4. The rack-cutter can also be set with some displacement values Δx_s, Δy_s, and Δz_s respect to the standard setting. As a result of the setting of the cutter with some of those magnitudes mentioned above, a modified pinion tooth surface may be obtained.

The purpose of generation of the pinion with a misaligned cutter is to be able to obtain a pinion tooth surface that will be conjugated to the wheel tooth surface when shaft deflections due to the design load are present. The misalignment of the wheel respect to the pinion is caused partially by shaft deflections. Magnitudes $\Delta\gamma_d$, $\Delta\nu_d$, Δx_d, Δy_d, and Δz_d, are obtained for the design load as it has been explained in previous section. These misalignment values will be considered as the settings for the generation of the pinion by its rack-cutter. In this way, the teeth of rack-cutter are in the same relative location respect to the pinion as the teeth of the misaligned wheel.

$$\begin{aligned} \Delta\gamma_s &= \Delta\gamma_d \\ \Delta\nu_s &= \Delta\nu_d \\ \Delta x_s &= \Delta x_d \\ \Delta y_s &= \Delta y_d \\ \Delta z_s &= \Delta z_d \end{aligned} \tag{8}$$

Additionally, the pinion tooth surface can be generated by cutter installed with misalignments and provided with modified profiles. In such a case, the pinion

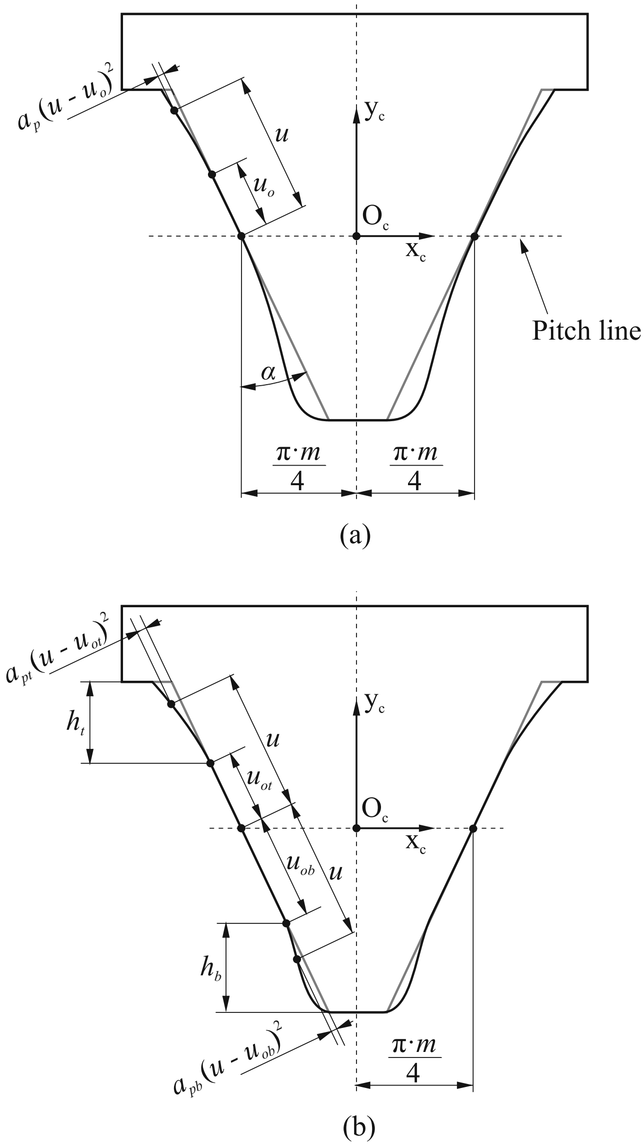

Fig. 5 Definition of the modified profiles of a rack-cutter for the application of (a) parabolic profile crowning and (b) parabolic relieves at top and bottom sides

tooth surfaces are modified by two actions, (i) the misaligned installment of the cutter, and (ii) the modified profiles of the cutter. Different types of profiles can be applied instead of the standard straight profile. Figure 5 shows two examples of definition of modified profiles in the normal section of a rack-cutter. Figure 5(a) shows the definition of a parabolic profile as the main active profile. A parabola is defined by the parabola coefficient a_p and the profile parameter u_o for the location of the parabola apex respect to the pitch line. Profile parameter u is measured along the straight reference profile whereas longitudinal parameter v is not shown in Fig. 5(a). Figure 5(b) shows another type of modified profile based on a straight profile and parabolic relieves at top and bottom sides. Parabola coefficients a_{pb} and a_{pt} are considered for definition of the parabolas at top and bottom sides, respectively. Parabola apexes are located by magnitudes u_{ot} and u_{ob} or, alternatively, by distances h_t and h_b.

4 Computerized simulation of gear meshing and determination of unloaded transmission errors

A general purpose algorithm has been applied for computerized simulation of gear meshing between pinion and wheel. It is based on a numerical method that takes into account the position of the surfaces and minimize the distances until contact is achieved, based on the work [14] and applied later in the works [15, 16]. This algorithm assumes rigid body behavior of tooth surfaces and can be applied to the analysis of gear drives in point, lineal, or edge contact. In the present work, no user defined misalignments will be considered for gear meshing investigation. The relation between the angle of rotation of the pinion, $\phi^{(1)}$, and the angle of rotation of the wheel, $\phi^{(2)}$, will provide the function of unloaded transmission errors, which will depend on the geometries of pinion and wheel tooth surfaces.

Transmission error is considered as the angular difference between the actual position of the wheel and the theoretical position of the wheel respect to the pinion. It is considered positive when the wheel moves away from the pinion and negative when the wheel moves towards the pinion. The function of unloaded transmission errors is obtained as the discrete function

$$\Delta\phi_i^{(u)} = \left(-\phi_i^{(2)} - \phi_i^{(1)}\frac{N_1}{N_2}\right) \tag{9}$$

where $\phi_i^{(1)}$ and $\phi_i^{(2)}$ are the angular rotations that allows pinion and wheel, respectively, to become in contact under no load at each contact position i. Here, superscript (u) means *unloaded*, N_1 and N_2 represents the number of teeth of pinion and wheel, respectively. The minus sign before angle $\phi_i^{(2)}$ is required since wheel rotation is considered negative in clockwise direction and $\phi_i^{(2)}$ makes the wheel to move away from the pinion.

5 Determination of load intensity functions and loaded transmission errors

Load intensity functions are determined considering the pressure distribution over the tooth surfaces obtained from the finite element analysis for each contact position. Details of determination of load intensity functions are described in [12]. Figure 6 shows an example

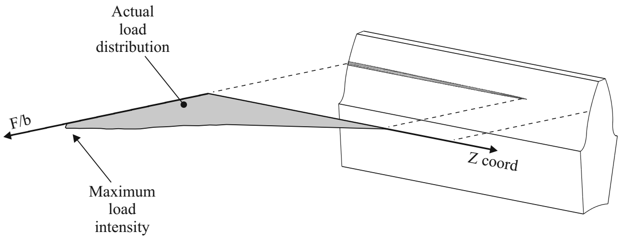

Fig. 6 Example of load intensity function along the face width for a bearing contact that is shifted

of a load intensity function when the bearing contact is shifted.

Loaded transmission errors are obtained for the whole cycle of meshing considering tooth bending deformations, contact deformations and torsional deformations of pinion and wheel. Torsional deformations of shafts are also considered. The procedure for the determination of the loaded transmission errors is as follows:

(i) Nodal rotations $\theta_i^{(P1)}$, $\theta_i^{(P2)}$, $\theta_i^{(W1)}$, and $\theta_i^{(W2)}$ at nodes $P1, P2, W1, W2$ are obtained at each contact position i from the finite element analysis.

(ii) Mean values of pinion and wheel rotations for each contact position are then obtained as

$$\overline{\theta}_i^{(p)} = \frac{\theta_i^{(P1)} + \theta_i^{(P2)}}{2} \tag{10}$$

$$\overline{\theta}_i^{(w)} = \frac{\theta_i^{(W1)} + \theta_i^{(W2)}}{2} \tag{11}$$

where $\overline{\theta}_i^{(p)}$ results positive when pinion shaft rotates in counterclockwise direction and $\overline{\theta}_i^{(w)}$ results negative when wheel shaft rotates in clockwise direction.

(iii) Since the nodal rotation of node $B2$ (see Fig. 2) is blocked, $-\overline{\theta}_i^{(w)}$ represents the wheel rotation due to torsional deformation of the wheel shaft between the end node $B2$ and the wheel location. The minus sign is required to make it positive, since the torsional deformation of the wheel shaft makes the wheel to move away from the pinion.

(iv) Since the pinion shaft is free to rotate, $\overline{\theta}_i^{(p)}$ represents the pinion rotation due to tooth contact deformations, tooth bending deformations, and torsional deformations of pinion and wheel. To account for all these deformations in the determination of the transmission error, $-\overline{\theta}_i^{(p)} \cdot N_1/N_2$ will represent the rotation of the wheel towards the pinion due to deformations. The minus sign is required to make it negative, since the deformations make the wheel to move closer to the pinion.

(v) Finally, the loaded transmission error is obtained as a discrete function by

$$\Delta\phi_i^{(l)} = \left(-\overline{\theta}_i^{(w)} - \overline{\theta}_i^{(p)}\frac{N_1}{N_2}\right) \tag{12}$$

Here, superscript l means *loaded*.

The torsional deformation of the pinion shaft between the end node $A2$ (see Fig. 2), where the torque is applied, and the pinion location, is not included in the determination of the loaded transmission error between pinion and wheel.

The set of results $\Delta\phi_i^{(l)}$ represents the function of loaded transmission errors. Such a function has to be added to the function of unloaded transmission errors $\Delta\phi_i^{(u)}$ to obtain the total function of transmission errors

$$\Delta\phi_i = \Delta\phi_i^{(u)} + \Delta\phi_i^{(l)} \tag{13}$$

The peak-to-peak transmission error is then defined as

$$\Delta\phi_{max} = \max(\Delta\phi_i) - \min(\Delta\phi_i) \tag{14}$$

The predesign of function $\Delta\phi_i^{(u)}$ may help reducing the value of $\Delta\phi_{max}$. This means that the predesign of the function $\Delta\phi_i^{(u)}$ may partially compensate the function $\Delta\phi_i^{(l)}$.

6 Numerical examples

Table 1 shows the main design data of the spur gear drive shown in Fig. 1. The gear drive is misplaced from the middle location between bearings by distances L_1 and L_2. The pinion is rotated in counterclockwise direction by the action of an applied torque T at bearing A_2 (see Fig. 2). A finite element model of 94211 elements and 121523 nodes has been considered.

Table 1 Design data of the spur gear drive represented in Fig. 1

Magnitudes	**Values**
Module, m [mm]	3.0
Pressure angle, α [degrees]	20.0
Tooth number of the pinion, N_1	34
Tooth number of the wheel, N_2	57
Face width, $b = b_p = b_w$ [mm]	25.0
Pinion shaft diameter, d_{sh1} [mm]	30.0
Wheel shaft diameter, d_{sh2} [mm]	35.0
Young's Modulus, E [MPa]	206800
Poisson's ratio, ν	0.29
Applied torque, T [Nm]	290.0
Distance *bearing A2 - pinion*, L_1 [mm]	100.0
Distance *pinion - bearing A1*, L_2 [mm]	40.0

A total of $i = 21$ contact positions are considered distributed along two cycles of meshing. In order to obtain shaft deflections, a standard geometry Σ_s of the pinion and a design load of $T = 290.0$ Nm are considered. For the determination of standard geometry Σ_s, a

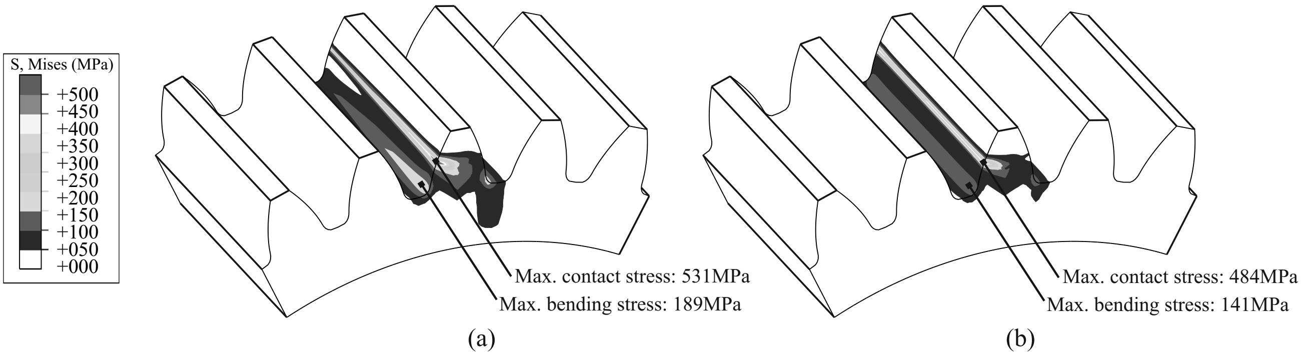

Fig. 7 Formation of the bearing contact and maximum contact and bending stresses at contact position 11 for (a) standard geometry Σ_s and (b) compensated geometry Σ_{c1}

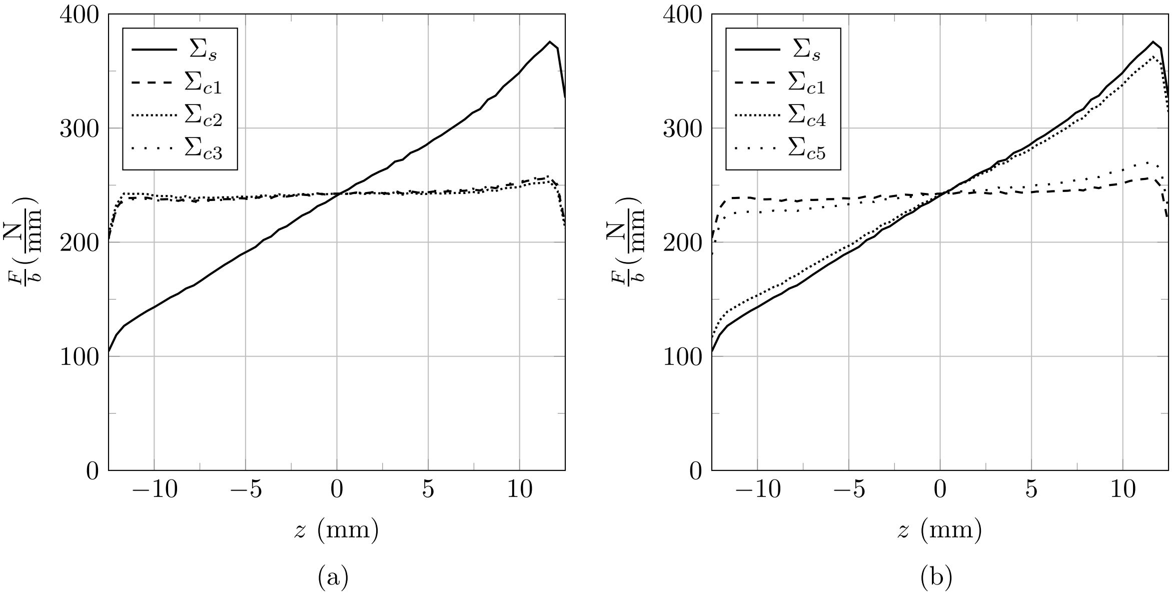

Fig. 8 Load intensity functions for standard geometry and compensated geometries at contact position 11: (a) comparison between Σ_s and Σ_{c1}, Σ_{c2}, and Σ_{c3}; (b) comparison between Σ_s and Σ_{c1}, Σ_{c4}, and Σ_{c5}

cutter with straight profiles installed in a standard setting (see Fig. 4(a)) is considered. Among the 21 contact positions, the maximum, minimum, and mean values of gear misalignments due to shaft deflections are obtained and shown in Table 2.

Table 2 Gear misalignments due to shaft deflections obtained for the standard geometry Σ_s and a torque of 290.0 Nm

	Max. values	Min. values	Mean values
$\Delta\gamma_d$[degrees]	-0,024266	-0,023326	-0,023551
$\Delta\nu_d$[degrees]	-0,008822	-0,008439	-0,008546
Δx_d[mm]	0,026187	0,025650	0,025776
Δy_d[mm]	-0,009536	-0,009311	-0,009378
Δz_d[mm]	0,0	0,0	0,0

Several compensated geometries of the pinion are then obtained by considering the gear misalignments shown in Table 2 as the settings for the installment of the cutter (see Section 3). For the obtention of these geometries, the cutter is provided with straight profiles. Five types of compensated geometries have been considered:

- Geometry Σ_{c1} is generated considering the mean values of gear misalignments shown in Table 2.
- Geometry Σ_{c2} is generated considering the maximum values of gear misalignments shown in Table 2.
- Geometry Σ_{c3} is generated considering the minimum values of gear misalignments shown in Table 2.
- Geometry Σ_{c4} is generated considering just the mean value of $\Delta\nu_d$ shown in Table 2.
- Geometry Σ_{c5} is generated considering just the mean value of $\Delta\gamma_d$ shown in Table 2.

Figure 7 shows the formation of the bearing contact on the pinion tooth surfaces at contact position 11 for geometries Σ_s and Σ_{c1} when a design load of $T = 290.0$

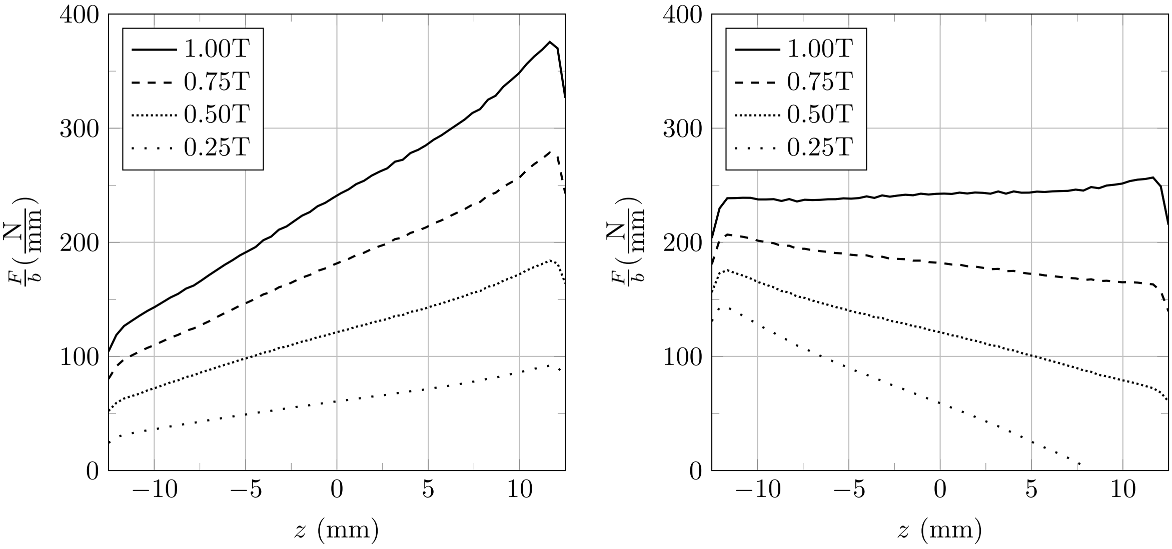

(a) (b)

Fig. 9 Load intensity functions at contact position 11 for several values of applied torque T = 290.0 Nm at (a) standard geometry Σ_s and (b) compensated geometry Σ_{c1}

Nm is applied. Figure 7(a) illustrates that the bearing contact is unevenly distributed and shifted towards the front face of the pinion when the standard geometry Σ_s is considered. However, when the compensated geometry Σ_{c1} is considered (see Fig. 7(b)), the bearing contact is uniformly distributed, providing a reduction on Mises contact stress about 8.85 percent and a reduction on Mises bending stress about 26.5 percent.

The standard geometry and the compensated geometries mentioned above are compared through the load intensity functions obtained at contact position 11. Figure 8(a) shows the load intensity functions for geometries Σ_s, Σ_{c1}, Σ_{c2}, and Σ_{c3}. The load intensity function provided by geometry Σ_s shows an important increment of the load intensity due to shaft deflections. However, the function provided by geometry Σ_{c1} shows an uniform distribution of the load intensity. Figure 8(a) shows as well that the load intensity functions provided by geometries Σ_{c1}, Σ_{c2}, and Σ_{c3} are very similar each other.

Figure 8(b) illustrates that the main contribution to get an uniform distribution of the load intensity and compensate the shaft deflections is due to magnitude $\Delta\gamma_d$, since the load intensity function provided by geometry Σ_{c5} is very close to the one provided by geometry Σ_{c1}. However, the load intensity function provided by geometry Σ_{c4} is very close to the one provided by geometry Σ_s, showing a minor influence of magnitude $\Delta\nu_d$ for compensation of shaft deflections.

Regarding the behavior of geometries Σ_s and Σ_{c1} when the load is different from the design load, Figure 9 illustrates the load intensity functions for both geometries and different values of the applied torque from $0.1T$ up to $1.0T$. The results show that under a low load, the load intensity is more uniformly distributed on the standard geometry Σ_s than on the compensated geometry Σ_{c1}. However and as it is expected, the load intensity becomes more uniformly distributed when the load is increased up to the design load for the compensated geometry Σ_{c1}.

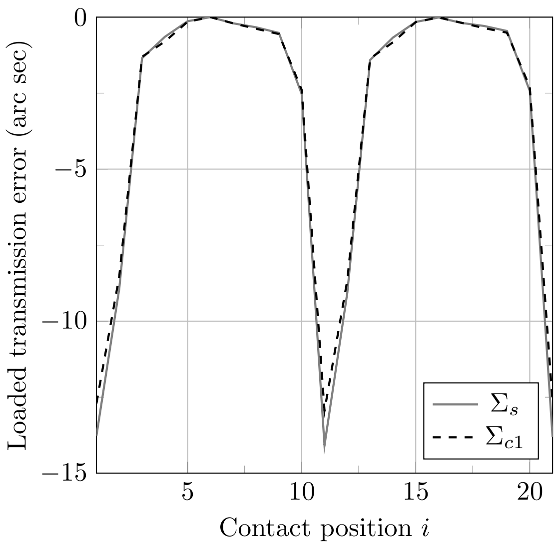

Fig. 10 Functions of loaded transmission errors for geometries Σ_s and Σ_{c1}

Regarding gear meshing results (see section 4), standard geometry Σ_s and compensated geometry Σ_{c1} provides a function of zero unloaded transmission errors due to the conjugated action between pinion and wheel

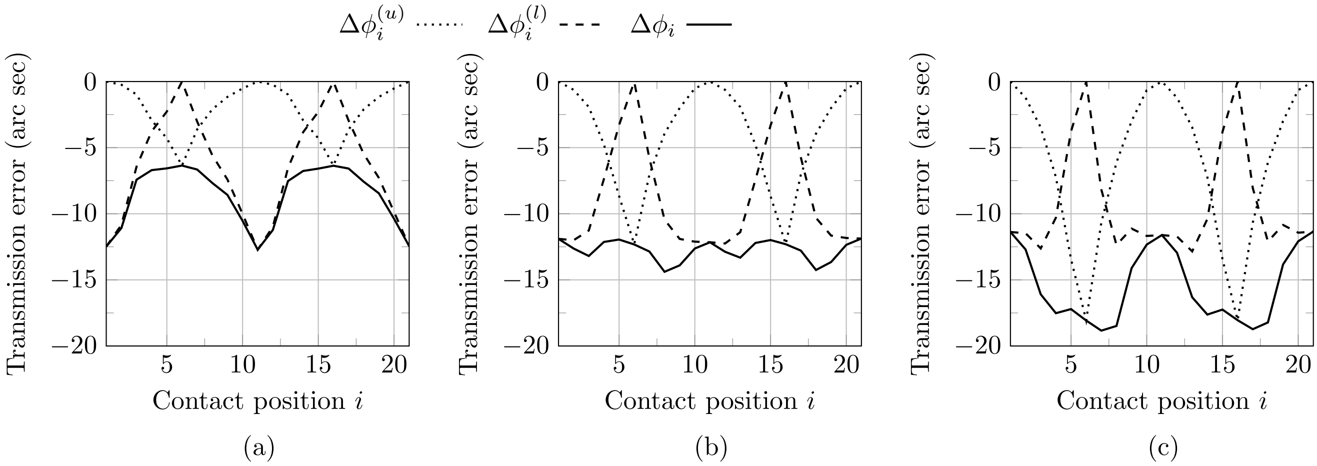

Fig. 11 Functions of transmission errors (unloaded, loaded, and total) for geometries: (a) Σ_{c1m1}, (b) Σ_{c1m2}, and (c) Σ_{c1m3}

tooth surfaces when no load is applied. The function of transmission errors is then obtained as the function of loaded transmission errors (see section 5). Figure 10 shows the functions of loaded transmission errors for geometries Σ_s and Σ_{c1}. Two cycles of meshing are observed. The peak-to-peak value of transmission error is about 14.08 arcsec for geometry Σ_s and 12.94 arcsec for geometry Σ_{c1}.

Several compensated modified geometries Σ_{c1mi} ($i = 1, \ldots, 11$) are generated for the investigation of the effect of the predesign of a function of unloaded transmission errors in the reduction of the peak-to-peak value of total transmission errors. Tables 3 and 4 show the main design parameters of the compensated modified geometries. Three compensated modified geometries are based on a whole crowning of the pinion tooth surfaces by application of a rack-cutter with parabolic profiles. Eight compensated modified geometries are based on a partial crowning of the pinion tooth surfaces by application of a rack-cutter with straight profile and parabolic relieves at bottom and top sides.

Table 3 Compensated modified geometries by application of whole crowning by parabolic profiles (see Fig. 5(a))

Geometry	a_p[mm^{-1}]	u_o [mm]
Σ_{c1m1}	0,001	-0,4
Σ_{c1m2}	0,002	-0,4
Σ_{c1m3}	0,003	-0,4

Figure 11 shows the functions of transmission errors (unloaded, loaded, and total) for geometries Σ_{c1m1}, Σ_{c1m2}, and Σ_{c1m3}. The lowest peak-to-peak value of total transmission errors is reached at geometry Σ_{c1m2}, representing such a geometry the best solution from the three considered geometries.

Table 4 Compensated modified geometries by application of partial crowning by parabolic relieves (see Fig. 5(b))

Geometry	a_{pt}[mm^{-1}]	h_t [mm]	a_{pb}[mm^{-1}]	h_b [mm]
Σ_{c1m4}	0,005	2,5	0,005	2,5
Σ_{c1m5}	0,010	2,5	0,010	2,5
Σ_{c1m6}	0,015	2,5	0,015	2,5
Σ_{c1m7}	0,020	2,5	0,020	2,5
Σ_{c1m8}	0,004	3,0	0,004	3,0
Σ_{c1m9}	0,008	3,0	0,008	3,0
Σ_{c1m10}	0,012	3,0	0,012	3,0
Σ_{c1m11}	0,016	3,0	0,016	3,0

Figure 12 shows the functions of transmission errors for geometries Σ_{c1m4}, Σ_{c1m5}, Σ_{c1m6}, and Σ_{c1m7} where $h_t = h_b = 2,5$ mm (see Fig. 5(b)). Figure 12(a) illustrates the increment of the peak-to-peak value of unloaded transmission errors when parabola coefficient is increased, whereas Figure 12(b) shows that the peak-to-peak value of loaded transmission errors is decreased due in part to the reduction of contact ratio. Figure 12(c) shows that the minimum peak-to-peak value of total transmission error is found for geometry Σ_{c1m5} from the four considered geometries.

Similar results can be found in Fig. 13 for compensated modified geometries Σ_{c1m8}, Σ_{c1m9}, Σ_{c1m10}, and Σ_{c1m11} where $h_t = h_b = 3,0$ mm. The minimum peak-to-peak value of total transmission error is found for geometry Σ_{c1m9} from the four considered geometries.

Regarding stress analysis results, it is important to notice that the developed research has been perform along two cycles of meshing and not just at one contact position. Figure 14 shows the evolution of contact and bending stresses for geometries Σ_s, Σ_{c1}, Σ_{c1m2}, Σ_{c1m5}, and Σ_{c1m9}. It is observed, along the cycle of meshing, a reduction of contact and bending stresses in the compensated geometries respect to the standard ge-

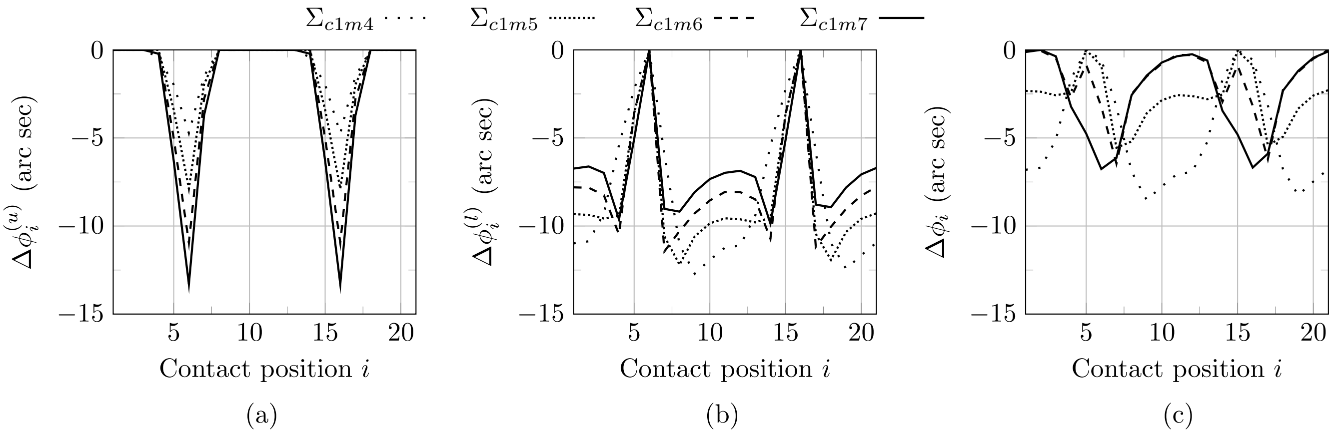

Fig. 12 Functions of (a) unloaded transmission errors, (b) loaded transmission errors, and (c) total transmission errors for geometries Σ_{c1m4}, Σ_{c1m5}, Σ_{c1m6}, and Σ_{c1m7}

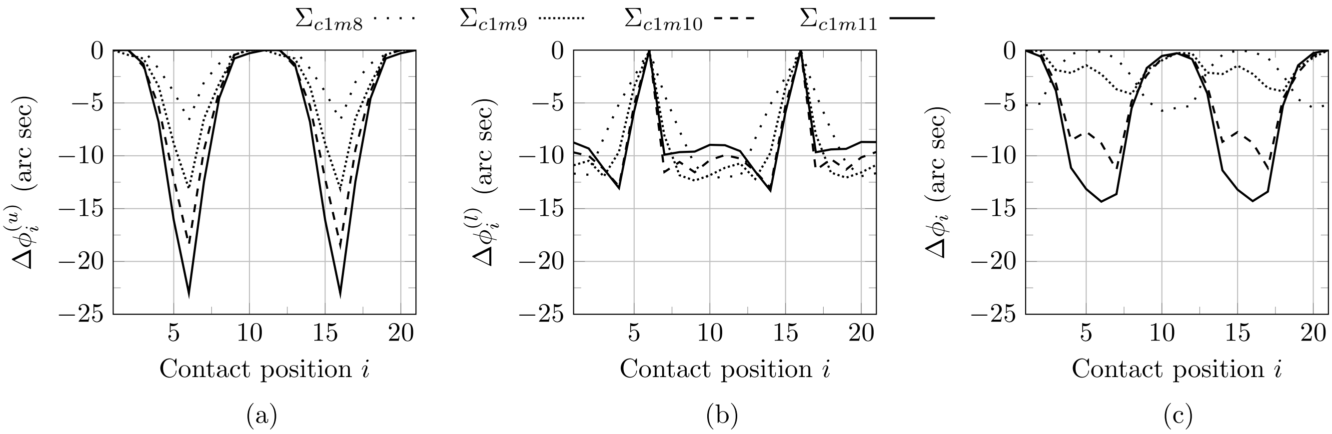

Fig. 13 Functions of (a) unloaded transmission errors, (b) loaded transmission errors, and (c) total transmission errors for geometries Σ_{c1m8}, Σ_{c1m9}, Σ_{c1m10}, and Σ_{c1m11}

ometry. Considering the modified compensated geometries, the profile crowning is even useful for elimination of some peaks on contact stresses due the rapid unload of teeth in contact. However the level of bending stresses is increased in modified compensated geometries respect to non-modified compensated geometries. The great advantage of modified compensated geometries is the reduction of the peak-to-peak transmission error (see Figs. 11, 12 or 13).

The evolution of the load intensity functions along the two cycles of meshing has also been investigated. Figure 15 shows the load intensity functions for all the 21 contact positions for geometries Σ_{c1} and Σ_{c1m2}. It is observed that compensation of shaft deflections is actually working for each contact position.

7 Conclusions and remarks

The developed research allows the following conclusions to be drawn:

1. A procedure for compensation of shaft deflections in gear generation has been proposed and provides a uniform distribution of load intensity between gear tooth surfaces for the design load at the driving side.
2. Compensation of shaft deflections in gear generation is complemented with the predesign of different types of unloaded functions of transmission errors that allows the peak-to-peak value of total transmission error to be reduced.
3. The developed research has been accomplished along two cycles of meshing to assure that the uniform distribution of load between gear tooth surfaces is actually kept along the cycle of meshing, and that the evolution of contact and bending stresses is satisfactory for the proposed geometries.

The developed research has been focus on the compensation of shaft deflections for a given pinion rotation direction, which means that the non-driving side of pinion teeth is sacrificed. In fact, a finite element analysis of the gear drive considering the contact at the non-

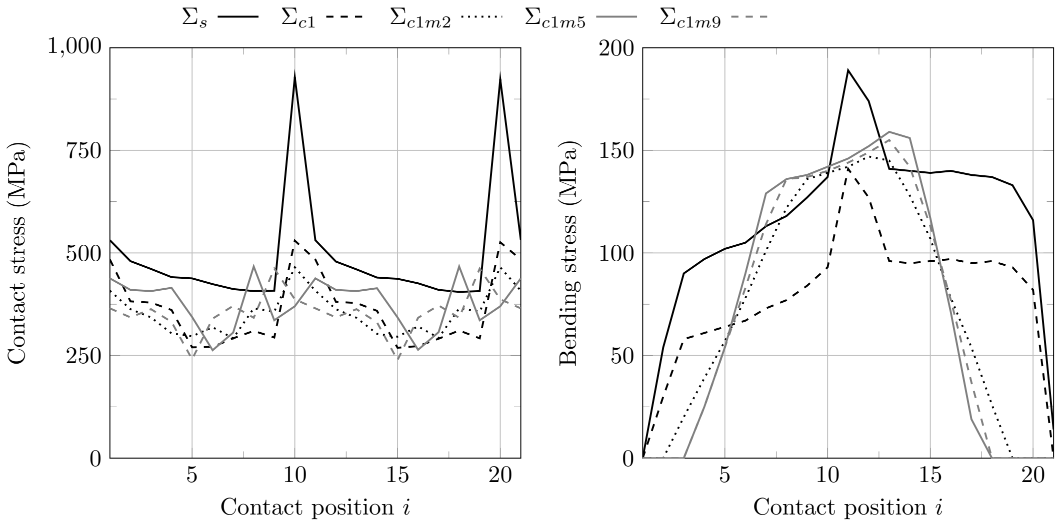

(a) (b)

Fig. 14 Evolution of stresses for geometries Σ_s, Σ_{c1}, and Σ_{c1m2}, Σ_{c1m5}, and Σ_{c1m9}: (a) contact Mises stresses, and (b) bending Mises stresses

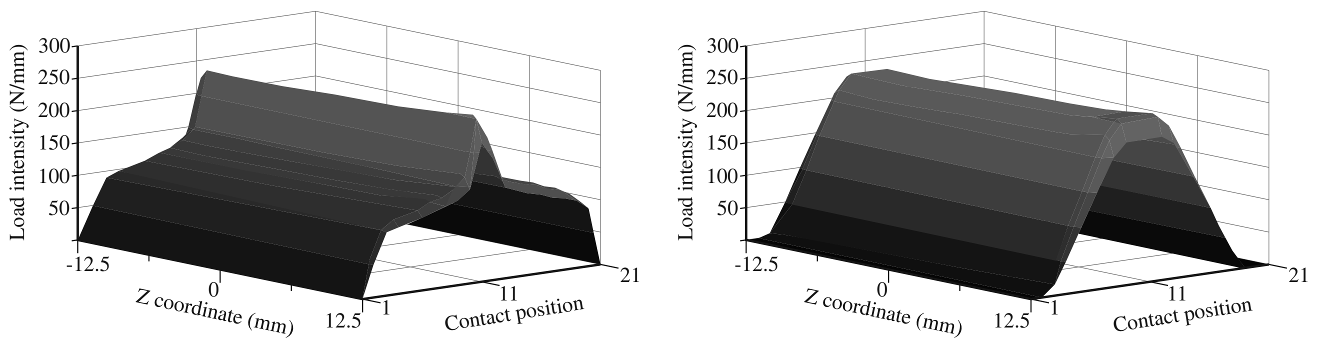

(a) (b)

Fig. 15 Load intensity functions along the cycle of meshing for geometries: (a) Σ_{c1} and (b) Σ_{c1m2}

driving side would provide an even worst load intensity function for the compensated geometries than for the standard geometry. Beside this, determination of backlash on the non-driving side is highly recommended for a better performance of the gear drive. All these topics are subject of future research.

Acknowledgements The authors express their deep gratitude to the Spanish Ministry of Economy and Competitiveness (MINECO) for the financial support of research project Ref. DPI2010-20388-C02-01 (financed jointly by FEDER) and DPI2010-20388-C02-02.

References

1. Harris SL (1958) Dynamic loads on the teeth of spur gears. Proc I Mech E 172(2):87–112
2. Gregory RW, Harris SL, Munro RG (1963) Dynamic behaviour of spur gears. Proc I Mech E 178(8):207–226
3. Optiz H (1968) Noise of gears. Phil Trans of the Royal Society 263:369–380
4. Bradley W (1973) How to design the noise out of gears. Machine Design 45(30):49
5. Welbourn DB (1979) Fundamental knowledge of gear noise - a survey. Proc Noise and Vibration of Engines and Transmissions, I Mech E, Cranfield, UK pp 9–14
6. Drago RJ (1980) How to design quiet transmissions. Machine Design pp 175–181
7. Wildhaber E (1962) Method and machine for producing crowned teeth. United States Patent Office, Patent No 3,046,844
8. Novikov ML (1956) Ussr patent no. 109,750
9. Litvin FL, Lu J, Townsend DP, Howkins M (1999) Computerized simulation of meshing of

conventional helical involute gears and modification of geometry. Mechanism and Machine Theory 34(1):123–147
10. Litvin FL, Fuentes A, Gonzalez-Perez I, Carnevali L, Kawasaki K, Handschuh RF (2003) Modified involute helical gears: Computerized design, simulation of meshing, and stress analysis. Computer Methods in Applied Mechanics and Engineering 192:3619–3655
11. Litvin FL, Gonzalez-Perez I, Fuentes A, Hayasaka K, Yukishima K (2005) Topology of modified surfaces of involute helical gears with line contact developed for improvement of bearing contact, reduction of transmission errors, and stress analysis. Mathematical and Computer Modelling 42(9-10):1063–1078
12. Gonzalez-Perez I, Roda-Casanova V, Fuentes A, Sanchez-Marin FT, Iserte JL (2012) A finite element model for consideration of the torsional effect on the bearing contact of gear drives. Journal of Mechanical Design 134(071007):1–8
13. Litvin FL, Fuentes A (2004) Gear Geometry and Applied Theory, 2nd edn. Cambridge University Press, New York (USA)
14. Sheveleva GI, Volkov AE, Medvedev VI (2007) Algorithms for analysis of meshing and contact of spiral bevel gears. Mechanism and Machine Theory 42(2):198–215
15. Fuentes A, Iserte JL, Gonzalez-Perez I, Sanchez-Marin FT (2011) Computerized design of advanced straight and skew bevel gears produced by precision forging. Computer Methods in Applied Mechanics and Engineering 200(29-32):2363–2377
16. Fuentes A, Ruiz-Orzaez R, Gonzalez-Perez I (2014) Computerized design, simulation of meshing, and finite element analysis of two types of geometry of curvilinear cylindrical gears. Computer Methods in Applied Mechanics and Engineering 272(0):321–339